

University of Nebraska - Lincoln DigitalCommons@University of Nebraska - Lincoln

Faculty Publications from Nebraska Center for
Materials and Nanoscience

Materials and Nanoscience, Nebraska Center for
(NCMN)

11-2015

Effect of Sm content on energy product of rapidly quenched and oriented SmCo₅ ribbons

Wenyong Zhang

University of Nebraska-Lincoln, wenyong.zhang@unl.edu


Xingzhong Li

University of Nebraska-Lincoln, xli2@unl.edu

Shah R. Valloppilly

University of Nebraska-Lincoln, svalloppilly2@unl.edu

Follow this and additional works at: <http://digitalcommons.unl.edu/cmrafacpub>

 Part of the [Atomic, Molecular and Optical Physics Commons](#), and the [Condensed Matter Physics Commons](#)

Zhang, Wenyong; Li, Xingzhong; and Valloppilly, Shah R., "Effect of Sm content on energy product of rapidly quenched and oriented SmCo₅ ribbons" (2015). *Faculty Publications from Nebraska Center for Materials and Nanoscience*. 121.
<http://digitalcommons.unl.edu/cmrafacpub/121>

This Article is brought to you for free and open access by the Materials and Nanoscience, Nebraska Center for (NCMN) at DigitalCommons@University of Nebraska - Lincoln. It has been accepted for inclusion in Faculty Publications from Nebraska Center for Materials and Nanoscience by an authorized administrator of DigitalCommons@University of Nebraska - Lincoln.

Effect of Sm content on energy product of rapidly quenched and oriented SmCo_5 ribbons

Wenyong Zhang, Xingzhong Li, and Shah Valloppilly

Nebraska Center for Materials and Nanoscience & Department of Physics and Astronomy, University of Nebraska–Lincoln, Lincoln, NE 68588, USA

Corresponding author — W. Zhang, email wenyong.zhang@unl.edu

Abstract

The Sm-content dependence of phase composition, anisotropy, and other magnetic properties of $\text{Sm}_{1+\delta}\text{Co}_5$ ($\delta \leq 0.12$) ribbons melt spun at 10 m/s has been studied. The samples consist of hexagonal SmCo_5 grains whose c axes are preferentially aligned along the long direction of the ribbon. The lattice parameter a and the cell volume (V) increase with increasing Sm content δ , whereas c decreases. Sm addition appears to improve the degree of the preferred orientation of the c -axis and to increase the mean grain size, which weakens the effective intergranular exchange coupling. Therefore, the remanence ratio, coercivity, and squareness of the hysteresis loops are significantly enhanced. The remanence ratio of 0.91 and the maximum energy product of 21.2 MGOe, which is the highest value reported so far for Sm–Co ribbons, are achieved for $\delta = 0.06$. High performance in combination with simple processing may facilitate high-temperature applications for anisotropic $\text{Sm}_{1+\delta}\text{Co}_5$ ribbons.

1 Introduction

SmCo_5 , which crystallizes in the CaCu_5 structure, has attracted much attention due to its giant magnetocrystalline anisotropy and high Curie temperature [1–3]. SmCo_5 materials are excellent candidates for high-temperature permanent magnets. Generally, the arc- and induction-melted SmCo_5 ingots have a very low coercivity because of large grain size (much larger than the critical single-domain size of 1.7 μm) and crystallographic isotropy. Surfactant-assisted ball milling (SABM) and

melt-spinning techniques are usually used to improve coercivity by decreasing grain size and developing c -axis texture. High coercivities of about 20 kOe were easily obtained for the anisotropic SmCo_5 nanoflakes by SABM [4–7]. However, some issues such as particle contamination, oxidation, wide size distribution, and complete removal of the surfactant limit the practical application of anisotropic SABM SmCo_5 nanoflakes. These problems are almost nonexistent for melt-spun SmCo_5 ribbons.

Melt spinning has been widely utilized to produce rare-earth transition-metal permanent magnets with high performance [8]. It was reported that the substitution of Ni for Co significantly increases the coercivity of $\text{SmCo}_{5-x}\text{Ni}_x$ ribbons at 30 m/s and led to the formation of c -axis orientation parallel to the length of the ribbon [9]. A c -axis alignment parallel to the ribbon was found for SmCo_5 ribbons at 6 m/s, which has $M_r/M_s = 0.80$, $H_c = 9.6$ kOe, and $(\text{BH})_{\text{max}} = 18.0$ MGOe [10]. Here, $M_r = 4\pi m_r$ is the remanent polarization; M_s is the saturation polarization; H_c denote the coercivity; and $(\text{BH})_{\text{max}}$ is the maximum energy product. As the wheel speed decreases to 5 m/s, M_r/M_s increases to 0.91, whereas H_c decreases to 3.2 kOe. A value of $(\text{BH})_{\text{max}} = 6.7$ MGOe was obtained for the SmCo_5 ribbons at 5 m/s [11]. The remanence of the Sm–Co ribbons at 5 m/s greatly increases with Sm content. But its coercivity only slightly increases [12], which limits the enhancement of energy product. The increase of wheel speed from 5 to 25 m/s leads to a rapid increase of H_c from 3.2 to 17.4 kOe for the SmCo_5 ribbons [11, 13]. Excessively high wheel speeds damage the texture of the ribbons and strongly reduce M_r/M_s . In this work, a wheel speed of 10 m/s was adopted. The effect of Sm content on structure and magnetic properties of $\text{Sm}_{1+\delta}\text{Co}_5$

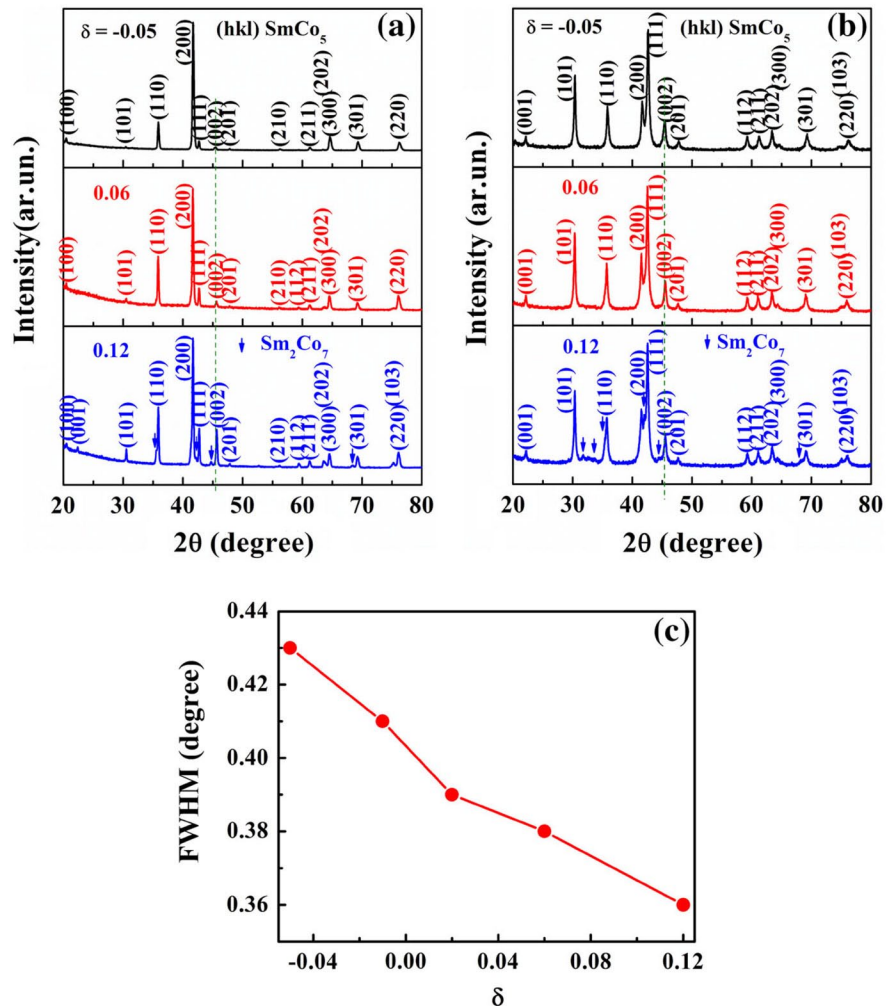
ribbons has been investigated, and high-coercivity SmCo_5 ribbons have been fabricated. An energy product of 21.2 MGOe has been achieved for $\delta = 0.06$. Then, an optimized Sm addition and wheel speed was found to significantly improve H_c , the hysteresis loop squareness, and $(BH)_{\max}$.

2 Experimental methods

Ingots with nominal composition of $\text{Sm}_{1+x}\text{Co}_5$ ($x = 0, 0.02, 0.05, 0.10, 0.15$) were arc melted from high-purity elements in an argon atmosphere. The ribbons were made by ejecting molten ingots in a quartz tube onto the surface of a copper wheel with a speed of 10 m/s. The process parameters such as ejection pressure (0.05–0.2 atm), diameter of the quartz tube hole (1–3 mm), melting time (1–3 min.), and distance (5–30 mm) between quartz tube and the surface of copper wheel were optimized for high-orientation ribbons. The length, width, and thickness of the ribbons for the magnetic measurements are

about 4, 2 mm, and 50 μm , respectively. The Co/Sm ratio was examined using energy dispersive X-ray (EDX) analysis attached to scanning electron microscopy (SEM). The real composition of $\text{Sm}_{1+x}\text{Co}_5$ ($x = 0, 0.02, 0.05, 0.10, 0.15$) has been determined to be $\text{Sm}_{15.97}\text{Co}_{84.03}$, $\text{Sm}_{16.53}\text{Co}_{83.47}$, $\text{Sm}_{16.94}\text{Co}_{83.06}$, $\text{Sm}_{17.49}\text{Co}_{82.51}$, $\text{Sm}_{18.30}\text{Co}_{81.70}$, respectively. It was concluded that the weight loss of Sm is about 5%. For the sake of simplicity, these compositions are written as $\text{Sm}_{1+\delta}\text{Co}_5$ ($\delta = -0.05, -0.01, 0.02, 0.06, 0.12$). The phase components were examined by Rigaku D/Max-B X-ray diffraction (XRD) system with $\text{Cu K}\alpha$ radiation. The phase content was determined by the TOPAS Rietveld analysis, and the nanostructure was observed by a Tecnai Osiris Transmission Electron Microscope (TEM). The magnetic properties were measured by a Quantum Design superconducting quantum-interference device (SQUID magnetometer) in fields of up to 7 T. The applied field was parallel to the length, width, or out-of-plane direction of the ribbons. The saturation magnetization M_s was determined using the law of approach-to-saturation to fit high-field part of $M(H)$ curves [14].

Figure 1. XRD patterns of
a) $\text{Sm}_{1+\delta}\text{Co}_5$ ($\delta = -0.05, 0.06, 0.12$) ribbons and
b) powdered $\text{Sm}_{1+\delta}\text{Co}_5$ ($\delta = -0.05, 0.06, 0.12$) ribbons;
c) full width at half maximum (FWHM) of the diffraction peak from (111) versus δ .



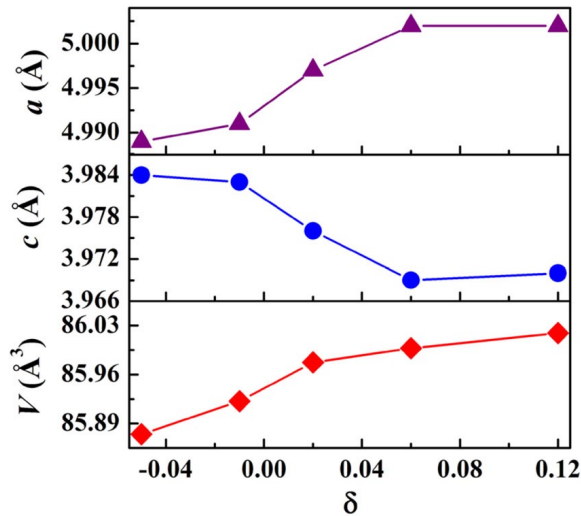


Figure 2. Lattice parameters a , c , and cell volume V of $\text{Sm}_{1+\delta}\text{Co}_5$ ribbons as a function of δ .

3 Results and discussion

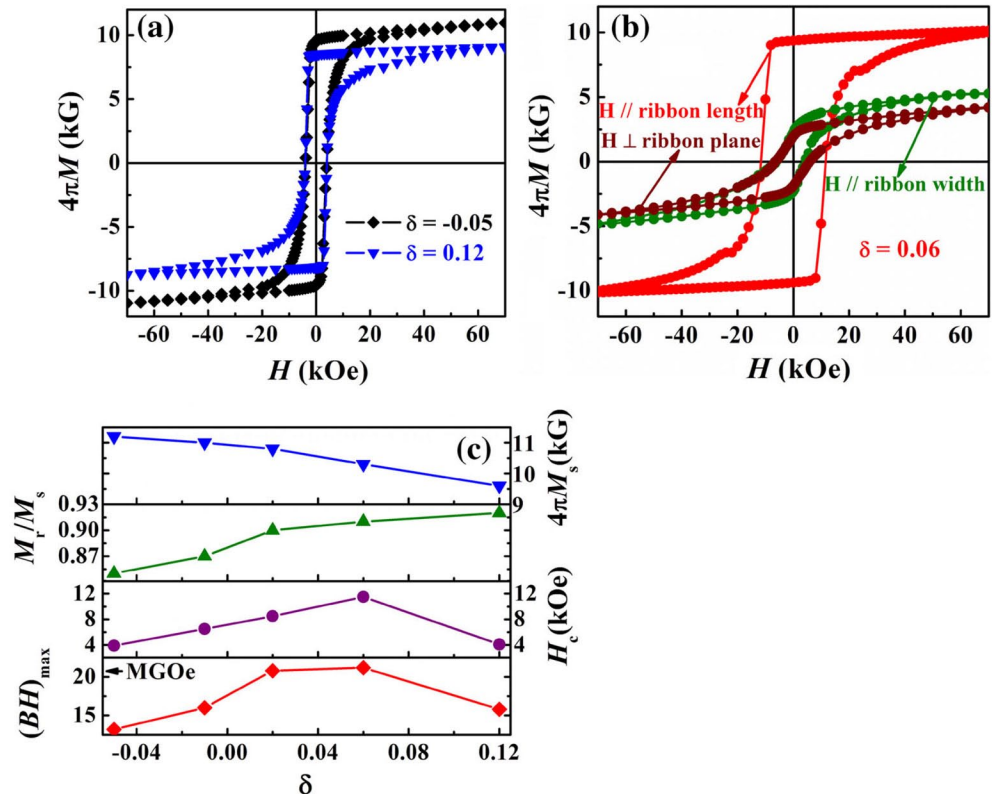
Figure 1a–c show XRD patterns of melt-spun $\text{Sm}_{1+\delta}\text{Co}_5$ ribbons, ribbon powders, and Sm-content dependence of full width at half maximum (FWHM) of the (111) diffraction peak. The ribbons with $\delta \leq 0.06$ consist of hexagonal SmCo_5 with the CaCu_5 structure. For the $\text{Sm}_{1+\delta}\text{Co}_5$ ribbons, the intensities of the (200)

reflection were the strongest, as compared for the (111) reflection, which is the strongest in isotropic SmCo_5 ribbon powders, as shown in Figure 1b. This indicates that the c -axis of the SmCo_5 grains primarily lies in the plane of the ribbons. For $\delta = 0.12$, some rhombohedral Sm_2Co_7 appears. Its volume fraction was determined by the Rietveld refinement to be 13%. The (002) peak shifts to higher angles with an increase of Sm content, indicating the decrease of lattice parameter c . The FWHM of diffraction peak from (111) shown in Figure 1b decreases with increasing δ . It qualitatively indicates that Sm addition increases the mean grain size of SmCo_5 .

Figure 2 shows Sm-content dependence of lattice parameters (a , c), cell volume (V) for the $\text{Sm}_{1+\delta}\text{Co}_5$ ribbons. Sm addition leads to an increase of a and a decrease of c . The V for the hexagonal structure is proportional to a^2c . The Sm concentration in homogeneity range for SmCo_5 phase at 1,260 °C is between 15.3 and 17.7 at.% [15]. High quenching rate is required to capture this high-temperature phase. The atomic radius of Sm (180 pm) is larger than that of Co (125 pm). Therefore, the V of SmCo_5 continuously expands with the increase in Sm content, which verifies the existence of the high-temperature homogeneity range for SmCo_5 . A similar tendency of change of lattice parameters with the variation of Sm content was observed in sintered SmCo_5 magnets [16, 17].

Figure 3a, b shows the hysteresis loops of $\text{Sm}_{1+\delta}\text{Co}_5$ in fields parallel to the ribbon ($\delta = -0.05$ – 0.12), in fields parallel to the width direction ($\delta = 0.06$), and in the out-of-plane direction,

Figure 3. Hysteresis loops of
a) the $\text{Sm}_{1+\delta}\text{Co}_5$ ($\delta = -0.05$ and 0.12) in a field parallel to the ribbon length direction,
b) $\delta = 0.06$ in a field parallel to the ribbon length direction, parallel to the width direction, and out-of-plane direction, and
c) deduced magnetization $4\pi M_s$, remanence ratio M_r/M_s , coercivity H_c , and maximum energy product $(BH)_{\max}$ versus δ .



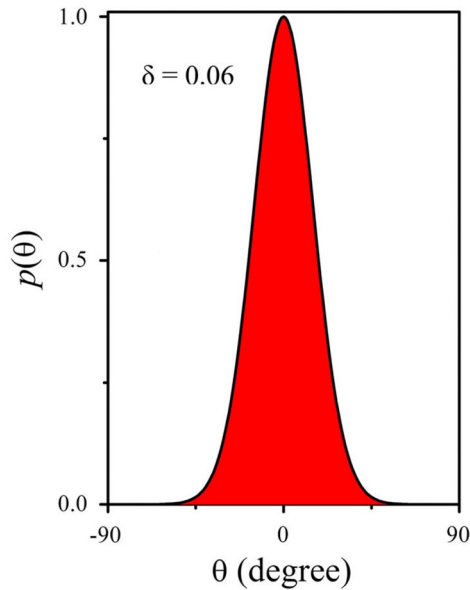


Figure 4. Normalized c -axis probability distribution function $p(\vartheta)$ for oriented SmCo_5 grains in the $\text{Sm}_{1+\delta}\text{Co}_5$ ($\delta = 0.06$) ribbon.

and Figure 3c summarizes the deduced magnetic properties. For $\delta = 0.06$, the magnetization, remanence, and coercivity along the length direction are much larger than those along the width and out-of-plane direction. This means that c -axis of the SmCo_5 phase in the ribbons aligns parallel to the length direction, in good agreement with the XRD results. We also see that the squareness of the demagnetization curve is significantly improved by the addition of a proper amount of Sm. The saturation magnetization M_s decreases with increasing Sm content. We believe that the magnetocrystalline anisotropy constant K does not change very much within the homogeneity range of SmCo_5 . Since the anisotropy field $H_a = 2K/M_s$, we conclude that H_a increases with increasing δ . The increase in H_a and in the mean grain size leads to an enhancement of the coercivity. Possible reasons for the nontrivial positive dependence of coercivity on grain size are due to the weakening of effective intergranular exchange coupling. H_c increases to a maximum value and then decreases possibly due to the formation of the

rhombohedral Sm_2Co_7 phase, which has a relatively low magnetocrystalline anisotropy.

It is known that, for low wheel speeds, the high temperature gradient along the radial direction of the copper wheel leads to the directional solidification of the SmCo_5 melt and to the formation of out-of-ribbon plane (200) texture/packed SmCo_5 crystal grains [10]. It is believed that the shear stress normal to the radial direction of the rotating copper wheel further induces the formation of preferred c -axis orientation parallel to the ribbon length direction. The addition of Sm may decrease the constitutional undercooling area and favor the growth of packed SmCo_5 crystallites. This leads to the enhancement of the degree of c -axis orientation, so the remanence ratio increases linearly with Sm addition. The maximum energy product increases with the Sm content due to the improvement of hysteresis loop squareness, coercivity, and remanence ratio. There is a small variation of the energy product between $\delta = -0.01$ and 0.06. This implies a wide composition window which is useful for the volume production of the melt-spun SmCo_5 with high performance.

For a non-interacting ensemble of uniaxial grains, the normalized average remanence can be written as [18]

$$M_n = \frac{M_r}{M_s} = \frac{\int M(\vartheta)p(\vartheta)\sin(\vartheta)d\vartheta}{\int p(\vartheta)\sin(\vartheta)d\vartheta} \quad (1)$$

where ϑ is the angle between the c -axis and field direction, and M is the normalized magnetic moment of the individual grains in the field direction. The c -axis distribution or texture function $p(\vartheta)$ can be approximated by

$$p(\vartheta) = p(0)\exp\left(\frac{\cos(\vartheta)}{\gamma}\right) \quad (2)$$

In this equation, γ parameterizes the width of the c -axis distribution ($\gamma \ll 1$ for good texture). For the $\delta = 0.06$ ribbon, $M_r/M_s = 0.91$ corresponding to a γ value of about 0.07 and to a narrow normalized c -axis distribution $p(\vartheta)/p(0)$, as shown in Figure 4. The percentage of SmCo_5 grains with alignment angles smaller than 25° is about 75 %.

Figure 5. In-plane-view TEM images of $\text{Sm}_{1+\delta}\text{Co}_5$ ribbons:

- a)** $\delta = 0.06$, the ribbon length direction and the c -axis indicated by yellow and white arrows, respectively and
b) $\delta = 0.12$, the Sm_2Co_7 phase being indicated by red arrows.

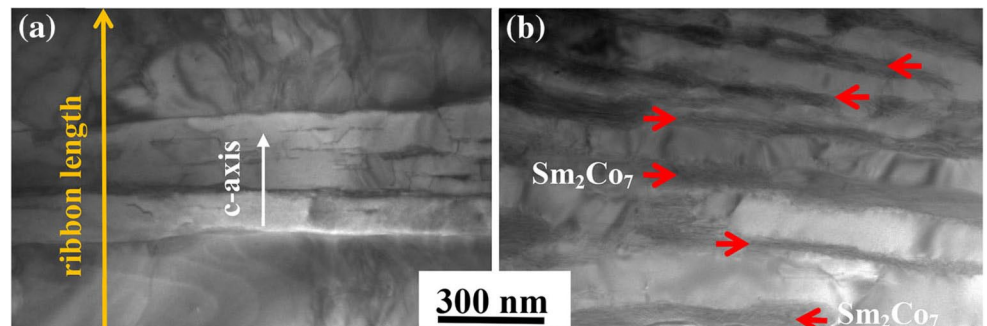


Figure 5 shows the TEM images of the $\text{Sm}_{1+\delta}\text{Co}_5$ samples with $\delta = 0.06$ and 0.12 . All the samples consist of tightly packed grains. EDX analysis reveals that the $\delta = 0.06$ sample is composed of the SmCo_5 phase, whereas the $\delta = 0.12$ sample consists of the SmCo_5 and Sm_2Co_7 regions, the latter being the gray stripes indicated by the red arrows. It is estimated that the volume fraction of the Sm_2Co_7 phase is 13 %. The above results are in good agreement with the XRD results. This confirms that most of the SmCo_5 grains exhibit *c*-axis alignment parallel to the long direction of the ribbons [19].

4 Conclusions

Highly anisotropic $\text{Sm}_{1+\delta}\text{Co}_5$ magnetic materials with large energy products have been fabricated by melt spinning. The ribbons ($\delta \leq 0.06$) consist of the single-phase hexagonal SmCo_5 and exhibit preferential *c*-axis parallel to the ribbon length direction. Proper Sm addition improves remanence, remanence ratio, and coercivity and thus increases the energy product. Excessive Sm addition leads to the formation of the Sm_2Co_7 phase, which deteriorates the magnetic properties. An energy product of 21.2 MGOe, which is the record value for Sm–Co ribbons, was achieved for the $\delta = 0.06$. The high performance, high Curie temperature, and simple processing suggest that melt-spun SmCo_5 may be useful for compacted or bonded high-temperature magnets.

Acknowledgments — This work is supported by US Department of Energy, Office of Basic Energy Science, Division of Materials Science and Engineering under Award No. DE-FG02-04ER46152. Electron microscopy research was supported by NSF-MRI (DMR-0960110). Research was performed in part in Facilities of the Nebraska Center for Materials and Nanoscience, which is supported by the Nebraska Research Initiative. We would like to thank Prof. David J. Sellmyer, Prof. R. Skomski, and Dr. B. Balasubramanian for the useful discussions.

References

1. K.J. Strnat, *Ferromagnetic Materials*, vol. 4, ed. by E.P. Wohlfarth, K.H.J. Buschow (Amsterdam: North-Holland, 1988), p. 131
2. O. Gutfleisch, *J. Phys. D Appl. Phys.* 33, R157 (2000)
3. C.B. Rong, N. Poudyal, X.B. Liu, Y. Zhang, M.J. Kramer, J. Ping Liu, *Appl. Phys. Lett.* 101, 152401 (2012)
4. N.G. Akdogan, G.C. Hadjipanayis, D.J. Sellmyer, *J. Appl. Phys.* 105, 07A710 (2009)
5. C.H. Chen, S.J. Knutson, Y. Shen, R.A. Wheeler, J.C. Horwath, P.N. Barnes, *Appl. Phys. Lett.* 99, 012504 (2011)
6. S.K. Pal, L. Schultz, O. Gutfleisch, *J. Appl. Phys.* 113, 013913 (2013)
7. Y.P. Wang, Y. Li, R.C. Rong, J.P. Liu, *Nanotechnology* 18, 465701 (2007)
8. S. Sugimoto, *J. Phys. D Appl. Phys.* 44, 064001 (2011)
9. J. Strzeszewski, G.C. Hadjipanayis, *J. Appl. Phys.* 67, 4595 (1990)
10. J. Ding, P.G. McCormick, R. Street, *J. Alloys Compd.* 228, 102 (1995)
11. A.R. Yan, W.Y. Zhang, H.W. Zhang, B.G. Shen, *J. Magn. Magn. Mater.* 210, L10 (2000)
12. A.R. Yan, W.Y. Zhang, H.W. Zhang, B.G. Shen, *J. Appl. Phys.* 88, 2787 (2000)
13. J.B. Sun, D. Han, C.X. Cui, W. Yang, L. Li, F. Yang, *Acta Mater.* 57, 2845 (2009)
14. G.C. Hadjipanayis, D.J. Sellmyer, *Phys. Rev. B* 23, 3349 (1981)
15. H. Okamoto, *J. Phase Equilib. Diffus.* 32, 165 (2011)
16. M.F. de Campos, F.J.G. Landgraf, *J. Phase Equilib.* 21, 443 (2000)
17. M.F. de Campos, F.J.G. Landgraf, N.H. Saito, S.A. Romero, A.C. Neiva, F.P. Missell, E. de Morais, S. Gama, E.V. Obrucheva, B.V. Jalnin, *J. Appl. Phys.* 84, 368 (1998)
18. B. Balasubramanian, B. Das, R. Skomski, W.Y. Zhang, J. David, J. Sellmyer *Adv. Mater.* 25, 6090 (2013)
19. L. Li, W.Y. Zhang, Y.Q. Zhou, J.Q. Li, B.G. Shen, J. Zhang, *Appl. Phys. Lett.* 80, 2660 (2002)